Systems/Circuits

Cell-Specific Activity-Dependent Fractionation of Layer 2/3→5B Excitatory Signaling in Mouse Auditory Cortex

Ankur Joshi,[1,2]* Jason W. Middleton,[1,2]* Charles T. Anderson,[1,2] Katharine Borges,[3] Benjamin A. Suter,[3] Gordon M. G. Shepherd,[3,4] and Thanos Tzounopoulos[1,2,4]

[1]Departments of Otolaryngology and [2]Neurobiology, University of Pittsburgh School of Medicine, Pittsburgh, Pennsylvania 15261, [3]Department of Physiology, Feinberg School of Medicine, Northwestern University, Chicago, Illinois 60611, and [4]Whitman Center, Marine Biological Laboratory, Woods Hole, Massachusetts 02543

Auditory cortex (AC) layer 5B (L5B) contains both corticocollicular neurons, a type of pyramidal-tract neuron projecting to the inferior colliculus, and corticocallosal neurons, a type of intratelencephalic neuron projecting to contralateral AC. Although it is known that these neuronal types have distinct roles in auditory processing and different response properties to sound, the synaptic and intrinsic mechanisms shaping their input–output functions remain less understood. Here, we recorded in brain slices of mouse AC from retrogradely labeled corticocollicular and neighboring corticocallosal neurons in L5B. Corticocollicular neurons had, on average, lower input resistance, greater hyperpolarization-activated current (I_h), depolarized resting membrane potential, faster action potentials, initial spike doublets, and less spike-frequency adaptation. In paired recordings between single L2/3 and labeled L5B neurons, the probabilities of connection, amplitude, latency, rise time, and decay time constant of the unitary EPSC were not different for L2/3→corticocollicular and L2/3→corticocallosal connections. However, short trains of unitary EPSCs showed no synaptic depression in L2/3→corticocollicular connections, but substantial depression in L2/3→corticocallosal connections. Synaptic potentials in L2/3→corticocollicular connections decayed faster and showed less temporal summation, consistent with increased I_h in corticocollicular neurons, whereas synaptic potentials in L2/3→corticocallosal connections showed more temporal summation. Extracellular L2/3 stimulation at two different rates resulted in spiking in L5B neurons; for corticocallosal neurons the spike rate was frequency dependent, but for corticocollicular neurons it was not. Together, these findings identify cell-specific intrinsic and synaptic mechanisms that divide intracortical synaptic excitation from L2/3 to L5B into two functionally distinct pathways with different input–output functions.

Key words: **auditory cortex; cortical mechanisms; intrinsic mechanisms; short-term plasticity; synaptic mechanisms**

Introduction

The corticocollicular projection from auditory cortex (AC) to the inferior colliculus (IC) plays crucial modulatory roles in auditory processing (Winer, 2006; Suga, 2012; Stebbings et al., 2014). The functional properties of the corticocollicular projection have been studied by electrically stimulating AC while measuring IC responses (Yan and Ehret, 2002; Yan et al., 2005; Suga, 2012). For example, AC stimulation enhances the responses of IC neurons that are matched in best-frequency to the AC-stimulated neuron, but suppresses IC responses that are unmatched (Suga, 2012). AC stimulation shifts the frequency tuning of IC neurons (Yan and Ehret, 2002), and modulates the gain of IC neurons' responses by elevating thresholds and reducing dynamic ranges (Yan and Ehret, 2002). Behavioral studies show that corticocollicular projections mediate learning-induced plasticity (Suga et al., 2002; Bajo et al., 2010). Whereas progress has been made toward characterizing AC→IC projections at the level of the IC (Doucet et al., 2003; Suga and Ma, 2003; Bajo et al., 2010), the intracortical circuits and cellular mechanisms shaping the activity of corticocollicular neurons remain incompletely understood.

Corticocollicular neurons in AC are located in L5B (Games and Winer, 1988; Doucet and Ryugo, 2003; Doucet et al., 2003; Slater et al., 2013). L5B also contains another major class of projection neurons, the corticocallosal neurons (Games and Winer, 1988). Corticocallosal neurons, which are found in other layers as well, project axons via the corpus callosum to the contralateral AC and thereby mediate interhemispheric connectivity between the right and left AC cortices (de la Mothe et al., 2006). Callosal projections are important in establishing a continuity of sensory representation across the two hemispheres (Hackett and Phillips, 2011).

Recent studies in a variety of cortical areas have revealed numerous differences in the physiological properties of pyramidal-

Received March 1, 2014; revised Dec. 21, 2014; accepted Jan. 10, 2015.

Author contributions: G.M.G.S. and T.T. designed research; A.J., J.W.M., C.T.A., K.B., and B.A.S. performed research; A.J., J.W.M., C.T.A., K.B., B.A.S., G.M.G.S., and T.T. analyzed data; G.M.G.S. and T.T. wrote the paper.

This work was supported by National Institutes of Health grants DC013272 (T.T. and G.M.G.S.), DC007905 (T.T.), NS061963 (G.M.G.S), R03DC012585 (J.W.M.), T32DC011499 (C.T.A.), and F32DC013734 (C.T.A), and by the Albert and Ellen Grass Faculty Award (T.T. and G.M.G.S.) and Charles Evans Foundation Award (T.T. and G.M.G.S.).

*A.J. and J.W.M. contributed equally to this work.

The authors declare no competing financial interests.

Correspondence should be addressed to Thanos Tzounopoulos, Departments of Otolaryngology and Neurobiology, University of Pittsburgh School of Medicine, Pittsburgh, Pennsylvania 15261. E-mail: thanos@pitt.edu.

J. W. Middleton's present address: Departments of Cell Biology and Anatomy, LSUHSC School of Medicine, New Orleans, LA 701112.

DOI:10.1523/JNEUROSCI.0836-14.2015

 0270-6474/15/353112-12$15.00/0

tract (PT) neurons, of which corticocollicular are a subtype, and intratelencephalic (IT) neurons, of which corticocallosal neurons are a subtype (for review, see Shepherd, 2013). While anatomical differences and differential response properties to sound have been reported for L5 PT and IT neurons in AC (Turner et al., 2005; Atencio and Schreiner, 2010a, b; Sun et al., 2013), the differences in synaptic and intrinsic properties of L5B PT and IT neurons and their contribution to the firing of L5B projection neurons have not been systematically studied in AC.

Here, we investigated the intrinsic and synaptic properties of corticocollicular and corticocallosal neurons with the general aim of characterizing the dynamic synaptic properties of these two major classes of infragranular neurons in mouse AC. We used *in vivo* retrograde labeling combined with *in vitro* electrophysiology-based methods. Our results indicate L5B AC neurons receive functionally distinct L2/3 input and exhibit different intrinsic properties. Together, these properties reveal an activity-dependent partition of L2/3→5B resulting in firing in corticocollicular neurons that is independent of the L2/3 stimulation rate, and in frequency-dependent, reduced firing in corticocallosal neurons at lower L2/3 stimulation rates.

Materials and Methods

Animals. ICR mice (Harlan; P22–P24 for microsphere injection and P24–P32 for recordings) of either sex were used for all experiments. All experimental procedures were approved by the Institutional Animal Care and Use Committee of the University of Pittsburgh.

Stereotaxic injections. Mice were anesthetized with isoflurane (induction: 3% in O_2, 0.6 L/min; maintenance: 50% of induction dose) and positioned in a stereotaxic frame (Kopf). Projection neurons in the AC were retrogradely labeled by injecting different colored fluorescent latex microspheres (Lumafluor) in the contralateral AC (in a small craniotomy drilled 4 mm posterior to bregma and 4 mm lateral, injection depth 1 mm) and the ipsilateral inferior colliculus (1 mm posterior to lambda and 1 mm lateral, injection depth 0.75 mm). A volume of ~0.1 μl microspheres was pressure injected (25 psi, 10–15 ms duration) from capillary pipettes (Drummond Scientific) with a Picospritzer (Parker–Hannifin). The injection volume was distributed between several sites along the injection depth to label the entire extent of the injection site. After injection, the pipette was held in the brain for 1.5 min before slowly withdrawing. The animals were allowed to recover for at least 48 hours to allow time for retrograde transport of the tracers.

In vivo *flavoprotein autofluorescence imaging.* Mice ($n = 11$) were anesthetized with urethane (induction: 1.5 mg/g; maintenance: 50% of induction dose). An incision (~1.5 cm) was made in the scalp and an intramuscular injection of lidocaine-epinephrine (2%) was delivered to the left temporal muscle. The temporal muscle was separated from the skull sufficiently to allow access to the underlying AC (~4.0–4.5 mm from the midline). The skull overlying the AC was thinned by careful drilling and left intact for transcranial flavoprotein autofluorescence (FA) imaging. Dental acrylic was used to secure a headpost to the skull over the ipsilateral frontal cortex and to create a reservoir for aCSF, which was periodically applied over the recording site to keep the skull from drying out. Subsequently, mice were head fixed and FA intrinsic signals were recorded while the animals were exposed to low-intensity auditory stimuli (amplitude-modulated tone with a carrier frequency of 5 KHz and modulation frequency of 20 Hz, 40–50 dB from speakers placed ~10 cm from the ear). The skull was exposed to blue light (LED light: peak wavelength = 461.4 nm; FWHM = 19.3 nm; M470L3; Thorlabs) for 10 s; 1 s acoustic stimuli were presented 3 s after initiation of exposure to blue light. During this time the endogenous FA signal (540 nm) was recorded by a CCD camera (Middleton et al., 2011). Two regions of sound-evoked FA activity were consistently observed: The more caudal of the two regions corresponds to the primary auditory cortex (A1) and the more rostral one corresponds to the anterior auditory field (AAF; Fig. 1). After FA imaging and AC identification a small piece of skull overlying the region identified as AC was exposed (by carefully scoring the perimeter of the thinned skull with a fine surgical blade and removing a small bone flap with fine forceps), and sulforhodamine was applied to the pial surface to label AC for *in vitro* identification experiments immediately after FA-assisted AC localization.

Slice electrophysiology. Coronal slices (300 μm) containing AC were prepared from mice that had previously been injected with retrograde beads and, in some experiments ($n = 5$, used for assessing intrinsic properties), had also undergone FA-assisted AC localization (see above and Results describing Fig. 1). The cutting solution, pH 7.35, contained the following (in mM): 2.5 KCl, 1.25 NaH_2PO_4, 25 $NaHCO_3$, 0.5 $CaCl_2$, 7 $MgCl_2$, 7 dextrose, 205 sucrose, 1.3 ascorbic acid, and 3 sodium pyruvate (bubbled with 95% O_2/5% CO_2). The slices were transferred and incubated at 36°C in a holding chamber for 30 min. The holding chamber contained aCSF, pH 7.35, containing the following (in mM): 125 NaCl, 2.5 KCl, 1.25 NaH_2PO_4, 25 $NaHCO_3$, 2 $CaCl_2$, 1 $MgCl_2$, 10 glucose, 1.3 ascorbic acid, and 3 sodium pyruvate (bubbled with 95% O_2/5% CO_2). Post incubation, the slices were stored at room temperature until the time of recording. Whole-cell recordings in voltage- and current-clamp modes were performed on slices bathed in carbogenated aCSF, which was identical to the incubating solution. The flow rate of the aCSF was ~1.5 ml/min, and its temperature was maintained at 32–34°C using an in-line heating system (Warner). To examine intrinsic properties, the following drugs were added to the aCSF (in mM): 0.02 DNQX (AMPA receptor antagonist), 0.05 APV (NMDA receptor antagonist), and 0.02 gabazine ($GABA_A$ receptor antagonist). Layer 5B of the AC was identified as the layer containing corticocollicular neurons. Recordings were targeted to either green fluorescent corticocollicular neurons or red fluorescent corticocallosal neurons within L5B. Borosilicate pipettes (World Precision Instruments) were pulled into patch electrodes with 3–6 MΩ resistance (Sutter Instruments) and filled with a potassium-based intracellular solution, which was composed of the following (in mM): 128 K-gluconate, 10 HEPES, 4 $MgCl_2$, 4 Na_2ATP, 0.3 Tris-GTP, 10 Tris phosphocreatine, 1 EGTA, and 3 sodium ascorbate. Data were sampled at 10 kHz and Bessel filtered at 4 kHz using an acquisition control software package Ephus (www.ephus.org; Suter et al., 2010). Pipette capacitance was compensated and series resistance for recordings was lower than 25 MΩ. Series resistance was determined in voltage-clamp mode (command potential set at −70 mV) by giving a −5 mV voltage step. Series resistance was determined by dividing the −5 mV voltage step by the peak current value generated immediately after the step in the command potential. These data were not corrected for 10 mV liquid junction potential. R_{input} was calculated in voltage-clamp mode (command potential set to −70 mV) by giving a −5 mV step, which resulted in transient current responses. The difference between baseline and steady-state hyperpolarized current (ΔI) was used to calculate R_{input} using the following formula: $R_{input} = -5\ mV/\Delta I - R_{series}$. The average resting membrane potential (V_m) was calculated by holding the neuron in voltage-follower mode (current clamp, at $I = 0$) immediately after breaking in and averaging the membrane potential over the next 20 s. Subthreshold and suprathreshold membrane responses in current clamp were elicited by injecting −200 to +500 pA in 50 pA increments (baseline V_m was maintained at −75 mV, by injecting the required current, if necessary). Sag was measured during the −200 pA current injection, using the formula, $SAG = (V_{min} - V_{steady\text{-}state})/V_{steady\text{-}state}$. The first resulting action potential (AP) at rheobase was analyzed for AP width. AP width was calculated as the full-width at the half-maximum amplitude of the AP. Adaptation ratio and fast-doublet index were measured at the current step that gave the closest AP firing rate to 10 Hz. Firing rate increases were quantified by calculating the initial (150–250 pA) slope of the frequency-current (*f–I*) relationship. We chose to calculate the slope between those three particular current points because they are above the nonlinear region of the curves near the rheobase, and they are below the region of large current values where the *f–I* functions start to saturate. Adaptation ratio was calculated by dividing the instantaneous frequency between the ninth and tenth AP by the instantaneous frequency between the second and third AP (f_9/f_2) (Fig. 4*H*,*K*). Fast-doublet index was calculated by dividing the instantaneous frequency between the first and second AP by the instantaneous frequency between the second and third AP (f_1/f_2; Fig. 4*F*,*H*,*I*,*L*). In Figures 3 and 4, which examine intrinsic properties,

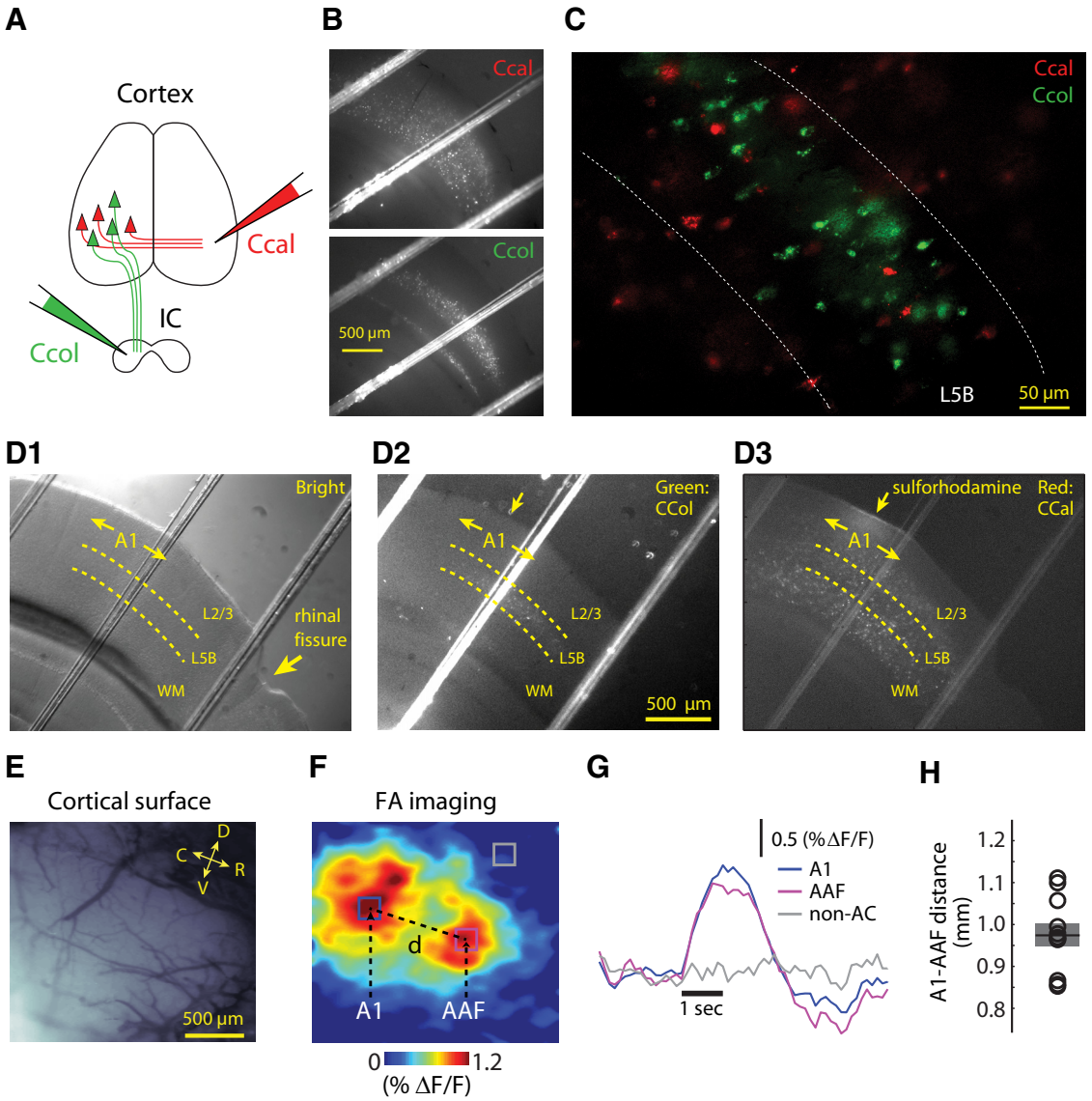

Figure 1. Localization and identification of AC corticocollicular (Ccol) and L5B corticocallosal (Ccal) neurons. ***A***, Labeling of corticocollicular and corticocallosal neurons with fluorescent tracers. Projection neurons in the AC were retrogradely labeled by injecting different colored fluorescent latex microspheres in the contralateral AC and the ipsilateral inferior colliculus. ***B***, Low magnification images (4×) show the full extent of AC and labeled Ccal (top) and Ccol neurons (bottom). ***C***, Merged image showing intermingling but no double labeling of corticocollicular (green) and corticocallosal (red) neurons in L5B of AC. ***D–H***, *In vivo* localization of AC areas by FA imaging of sound-evoked activity was performed in 11 experiments. ***D1–D3***, Bright-field (D1), green (D2), and red (D3) fluorescent images of a representative coronal slice that was labeled *in vivo* with sulforhodamine. The bright-field image (***D1***) indicates the rhinal fissure and the location of primary auditory cortex estimated from the stereotaxic coordinate mouse brain atlas (Franklin and Paxinos, 2001). The green fluorescent image (***D2***) shows retrogradely labeled corticocollicular neurons in L5B that are present in A1 and extend toward the rhinal fissure. The red fluorescent image (***D3***) shows the *in vivo* applied sulforhodamine spot. Sulforhodamine was applied to the pial surface *in vivo* and here identifies A1 in this coronal brain slice (FA-assisted A1 identification was performed as shown in ***E*** and ***F***). ***D3*** also shows retrogradely labeled corticocallosal neurons that extend medially and laterally from A1. The upper and lower layer 5B boundaries are indicated by dashed lines (WM stands for white matter). ***E***, Image of cortical surface indicating caudal (C), rostral (R), dorsal (D), and ventral (V) direction. ***F***, In response to amplitude-modulated tones (carrier frequency of 5 kHz and modulation frequency of 20 Hz, 40–50 dB), FA image shows peaks of activity corresponding to A1 and non-A1 auditory cortical areas. The more caudal (left) of the two domains of activation is A1 and the more rostral (right) of the two domains is the AAF. Image is an average of 10 trials and is from a frame taken 1 s after stimulus onset. Images were smoothed using a spatial filter with a 100 μm space constant. ***G***, The average (10 trials) relative fluorescence from regions of interest at the peak of A1 (blue) and AAF (magenta) area. The horizontal bar indicates the duration of the auditory stimulus. ***H***, The distance between the centers of 5 kHz activation of A1 and AAF (974 $\pm$ 27 μm, $n = 11$).

24/32 corticocollicular and 24/29 corticocallosal neurons were recorded from the same slice.

Paired recordings. Whole-cell recordings were established from a L2/3 neuron and a bead-labeled corticocollicular or L5B corticocallosal neuron. For these experiments, we used coronal slices without dye in the pipettes and therefore without direct assessment of intactness of dendritic arbors. Connectivity was assessed by evoking a train (five pulses, 20 Hz) of action potentials in the L2/3 neuron while monitoring the postsynaptic response in the L5B neuron; at least 20 trials of the presynaptic train were delivered (10 s intertrial interval); multiple trials were averaged to detect the presence of a connection. Events that were >3 SDs of the baseline noise level (noise levels were measured during a 50 ms timing period before the first spike in the presynaptic neuron) were classified as synaptic inputs and further analyzed. EPSC or EPSP latency was calculated as the time from the peak of the presynaptic AP to the time where the postsynaptic signal was >3 SDs of the baseline noise level. EPSC or EPSP amplitudes were obtained by averaging a 1 ms window around the peak response. Rise time was defined as the time from 20 to 80% of the peak response. Decay time constants were measured by fitting an exponential function from peak of a single EPSP to its baseline response. EPSC or EPSP trains were normalized to the amplitude of the first EPSC or EPSP before analyzing them for short-term plasticity. In current-clamp

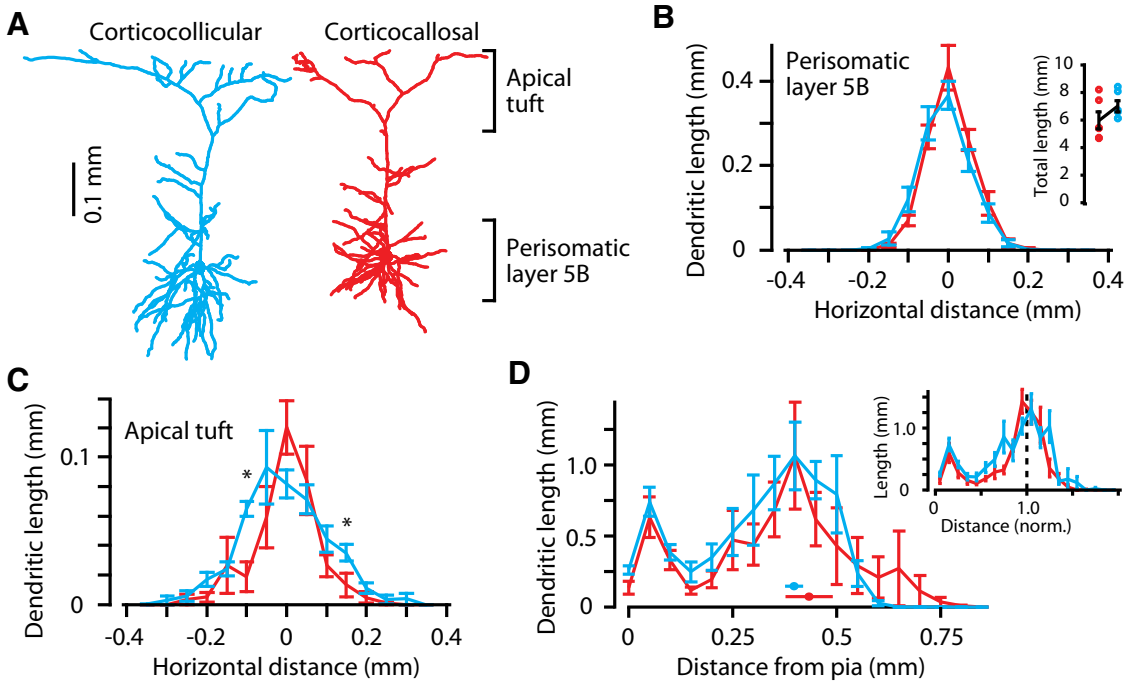

Figure 2. Dendritic morphology of corticocollicular and corticocallosal neurons in L5B of AC. ***A***, Example reconstructions. ***B***, Horizontal profile of the total dendritic length in the perisomatic/L5B region, showing the mean ± SEM for corticocollicular (blue; $n = 6$) and corticocallosal (red; $n = 6$) neurons. Each neuron's horizontal profile was calculated as the average in a 150 μm wide band extending horizontally across the perisomatic region, as indicated in ***A***. No significant differences were found at any of the locations (rank sum test). Inset, Total dendritic length, plotted as the mean ± SEM for the two cell types (lines) along with the individual values (circles). The samples were not significantly different (rank sum test). ***C***, Horizontal profile of the dendritic length in the apical tuft, showing the mean ± SEM for corticocollicular (blue; $n = 6$) and corticocallosal (red; $n = 6$) neurons. Each neuron's horizontal profile was calculated as the average in a 150 μm wide band extending horizontally across the apical tuft region, as indicated in ***A***. Locations where values differed significantly are marked with an asterisk ($p < 0.05$, rank sum test). ***D***, Vertical profiles, calculated as the dendritic length in 50 μm bins and plotted as the mean ± SEM for the two cell types; no differences were found (rank sum test). Inset, Each profile was first normalized to the soma (distance = 1), rebinned, and plotted as the mean ± SEM; no differences were found (rank sum test).

mode recordings, neurons were held at −75 mV. For 12 of 14 L2/3→corticocollicular connected pairs and for 9 of 11 L2/3→corticocallosal pairs, both EPCSs and EPSPs were recorded from the same postsynaptic neuron. With the exception of two paired recordings, we were not able to obtain more than one pair per slice.

Extracellular L2/3 stimulation and postsynaptic spiking experiments. Whole-cell recordings were established from bead-labeled corticocollicular or L5B corticocallosal neurons from the same slice; L2/3 was stimulated with a theta glass-stimulating electrode filled with extracellular solution. The stimulation electrode was positioned in L2/3, ~200 μm from the pial surface, and laterally to the recording electrode in L5B to avoid direct stimulation of L5B neurons. EPSCs were obtained while holding the neuron at −70 mV. EPSPs were obtained in current-clamp mode (membrane potential maintained at −75 mV for both cell types). To examine the effect of stimulation frequency on the firing of corticocallosal or to corticocollicular neurons, we adjusted the stimulus intensity such that in response to a stimulus train of 10 pulses at 20 Hz, ~50% spikes were evoked in the postsynaptic corticocallosal or corticocollicular neuron. Two stimulus trains (10 pulses in each train) were delivered for each frequency in the following order: 20, 10, and 20 Hz (intertrain interval: 10 sec). The spikes evoked by the two trains were averaged; i.e., we averaged the number of spikes evoked by trains 1 and 2 (20 Hz), the number of spikes evoked by trains 3 and 4 (10 Hz), and the number of spikes evoked by trains 5 and 6 (20 Hz). A trial was considered complete if the average number of spikes evoked in trains 5 and 6 did not change by >20% compared with the average spikes evoked in trains 1 and 2. For each neuron, the average number of spikes per frequency was normalized to the average number of spikes of the first two trains at 20 Hz. All recordings from the two different neuronal types were performed from the same slice.

Morphological reconstructions. As described in detail previously (Suter et al., 2013), neurons were filled with biocytin during whole-cell recordings, and the slices were fixed, processed for streptavidin-based fluorescent labeling, and imaged by two-photon microscopy. For morphological reconstructions, the angle of cutting was slightly modified for optimal preservation of dendritic arbors. Dendrites were three-dimensionally traced in stitched image stacks (Neurolucida) and datasets were further analyzed to quantify dendritic length as previously described (Shepherd et al., 2005; Yamawaki et al., 2014).

Statistical analysis. Data that were normally distributed (based on Lilliefors test) were analyzed using unpaired *t* tests. For non-normally distributed data, we used the Wilcoxon rank sum test (indicated wherever this was the case). Within-group analysis for paired recordings was done using paired *t* tests. Significance was reported if *p* value <0.05.

Results

Identification of corticocollicular and corticocallosal neurons in AC

To label corticocollicular and corticocallosal projection neurons in L5B of AC for subsequent targeted recordings in brain slices, we performed *in vivo* injections of fluorescent retrograde tracers. Small volumes of fluorescent microspheres were injected in the IC, while microspheres of different colors were injected in the contralateral AC (Fig. 1*A*). In brain slices prepared 2–3 days later, corticocollicular and corticocallosal neurons were selectively labeled (Fig. 1*B*,*C*). Consistent with previous studies of similar classes of projection neurons in A1 and in other cortical areas (Games and Winer, 1988; Akintunde and Buxton, 1992; Morishima and Kawaguchi, 2006), we found no double labeling (0 of >660 neurons) of these two populations; that is, this labeling paradigm labels two types of L5B projection neurons that represent distinct, nonoverlapping classes (Fig. 1*C*).

While AC is stereotaxically localizable in the intact brain, AC localization is more challenging in brain slices because its areal

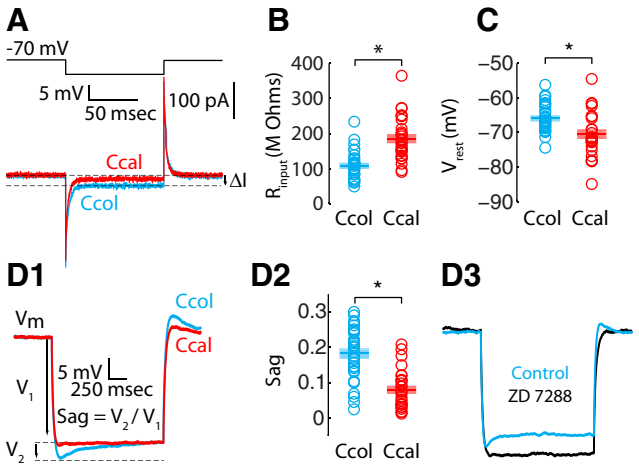

Figure 3. Intrinsic subthreshold properties of AC corticocollicular (Ccol) and L5B corticocallosal (Ccal) neurons are distinct. ***A***, Hyperpolarizing pulses (top) in voltage-clamp recording mode result in transient current responses (bottom). The difference between baseline and steady-state hyperpolarized current (ΔI) is used to calculate the input resistance of Ccol and Ccal neurons. ***B***, The average input resistance is significantly lower for Ccol neurons (108.11 ± 7.06 MΩ, $n = 32$ vs 185 ± 11.27 MΩ, $n = 29$; $p < 0.0001$). ***C***, The average resting membrane voltage, V_m, is significantly more depolarized for Ccol neurons (−65.98 ± 0.70 mV, $n = 32$ vs −70.54 ± 1.22 mV, $n = 29$; $p = 0.0014$). ***D1***, Hyperpolarizing current injection reveals sag potentials in Ccol and Ccal neurons. Sag is measured by dividing the difference between the minimum voltage hyperpolarization and the steady-state hyperpolarized voltage. ***D2***, The average sag is significantly higher for Ccol neurons (0.18 ± 0.01, $n = 32$, vs 0.08 ± 0.01, $n = 20$; $p < 0.0001$). ***D3***, Sag potentials are abolished by ZD7288 (black trace) indicating that they are mediated by hyperpolarization-activated cyclic nucleotide-gated channels (average sag in control = 0.10 ± 0.01; post-ZD7288 = 0.01 ± 0.01, $n = 3$, $p < 0.01$).

borders are not sharply demarcated by cytoarchitectural features. In general, in this study we were guided by (1) anatomical landmarks such as the rhinal fissure and underlying hippocampal anatomy (Fig. 1*D1*) and (2) the presence of retrogradely labeled neurons projecting to the inferior colliculus in localizing AC in slices (Fig. 1*D2*) as well as retrogradely labeled neurons projecting to the contralateral auditory cortex (Fig. 1*D3*). However, in the early phase of these studies we additionally localized the AC *ex vivo* using a two-step procedure that was based on a functional assay *in vivo*. First, we localized AC *in vivo* by transcranially measuring FA signals elicited by acoustic stimulation (Fig. 1*E–G*), and then we labeled AC identified by FA imaging with sulforhodamine (Fig. 1*D3*; Takahashi et al., 2006). FA signals are generated by mitochondrial flavoproteins due to changes in oxidation state caused by neuronal activity (Shibuki et al., 2003; Middleton et al., 2011). Mirror-reversed tonotopic gradients have been used to identify A1 and the AAFs in many mammalian species including mice (Kaas, 2011; Guo et al., 2012). In response to low-frequency sound (5 kHz), we observed two distinct regions with increased FA activity, representing the caudal end of A1 and the rostral end of AAF (Fig. 1*E*). The relative location of the FA signals (Fig. 1*F*), the timing of the FA signals after the stimulus onset (Fig. 1*G*), and the distance (Fig. 1*H*) between the centers of two regions of the FA signals are consistent with localization of mouse A1 using FA, electrophysiological recordings, or optical Ca^{2+} imaging (Stiebler et al., 1997; Takahashi et al., 2006; Guo et al., 2012; Honma et al., 2013; Issa et al., 2014). After completion of FA-assisted localization of A1, we applied a fluorescent dye to mark the location of A1 (Lefort et al., 2009), enabling us to precisely localize the A1 region of AC in subsequently prepared brain slices (Fig. 1*D*). These results suggest that FA- and sulforhodamine-assisted A1 localization is an efficient approach for localizing A1 in brain slice recordings. The FA- and sulforhodamine-assisted A1 localization helped us to localize A1 in the initial phase of the project. Because these experiments revealed that the location of A1 was consistent in relation to the location of retrogradely labeled corticocollicular neurons, in subsequent experiments, we relied on retrograde labeling of corticocollicular neurons and on the rhinal fissure and underlying hippocampal anatomy for targeting our recordings to AC.

To characterize the dendritic morphology of corticocollicular and corticocallosal neurons we filled them with biocytin to reconstruct their dendritic arbors. Both cell types displayed the morphological hallmarks of cortical pyramidal neurons, with numerous branches in the basal perisomatic arbor and a prominent apical dendrite extending to the pia, branching into an apical tuft in L1 (Fig. 2*A*). Neither the total dendritic length (Fig. 2*B*, inset) nor the amount and horizontal spread of dendrites in the L5B perisomatic region (Fig. 2*B*) differed between the two cell types ($n = 6$ corticocollicular, $n = 6$ corticocallosal; $p > 0.05$, rank sum test). However, compared with corticocallosal neurons, corticocollicular neurons had more horizontally spreading apical tufts in layer 1 (Fig. 2*C*). The vertical profiles of dendrites (dendritic length as a function of absolute or soma-normalized depth) did not differ significantly between corticocallosal and corticocollicular neurons (Fig. 2*D*). These results indicate that the differences in dendritic structure between the two cell types are primarily in the distal dendritic arbors in the apical tufts but not in their basal arbors. These results appear broadly consistent with, but smaller in magnitude, than the reported morphological differences of putative PT and IT neurons in rat AC (Sun et al., 2013) and with prior reports for IT and PT neurons in other cortical areas and species (Gao and Zheng, 2004; Dembrow et al., 2010).

Intrinsic properties of L5B projection neurons

To characterize the intrinsic properties of the two classes of projection neurons, labeled corticocollicular and L5B corticocallosal neurons were targeted for whole-cell recordings in voltage- and current-clamp modes. Corticocollicular neurons, compared with corticocallosal neurons, had lower input resistance (Fig. 3*A*,*B*), depolarized resting membrane potential (Fig. 3*C*), and greater "sag potentials" in response to hyperpolarizing pulses (Fig. 3*D1*,*D2*). Sag potentials were abolished by 10 μM ZD7288 (an I_h blocker; Fig. 3*D3*) suggesting that I_h mediates these potentials. These results are consistent with previous studies of corresponding classes of projection neurons in auditory, motor, and prefrontal cortex (Dembrow et al., 2010; Sheets et al., 2011; Shepherd, 2013; Slater et al., 2013; Suter et al., 2013).

Next, we evaluated the spike-related properties of corticocollicular and corticocallosal neurons in L5B. Corticocollicular neurons displayed faster action potentials (Fig. 4*A*,*B*). Moreover, the action potential threshold of corticocollicular neurons was more hyperpolarized (Fig. 4*C*). In response to depolarizing current, repetitive firing patterns differed (Fig. 4*D*). The initial linear slope of the current-firing frequency (*f–I*) function revealed that firing rate increased faster in corticocollicular neurons (Fig. 4*E*,*F*); moreover the *f–I* function revealed that the threshold for eliciting firing was higher for corticocollicular neurons (Fig. 4*E*,*G*). Corticocollicular neurons often fired faster initial doublets (Fig. 4*I*,*L*, inset) at the onset of current injection while corticocallosal neurons do not (Fig. 4*I*,*L*). Spike frequency decreased (adapted) over time in corticocallosal neurons while it remained nearly constant in corticocollicular neurons (Fig. 4*I*,*K*). Initial instantaneous frequency for corticocollicular neurons was high (Fig. 4*J1*), reflecting more fast-doublet firing. The

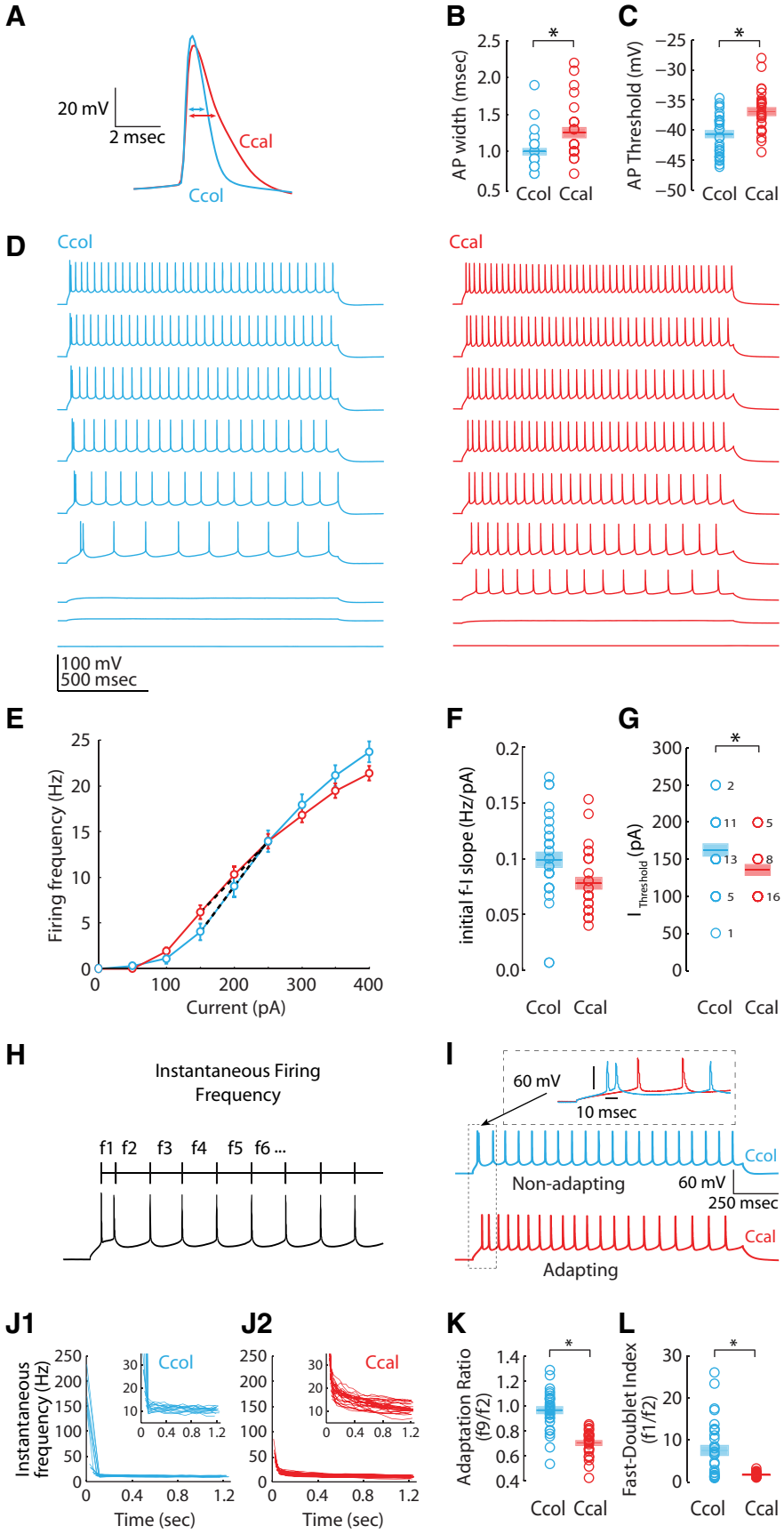

Figure 4. AP properties and spike-frequency adaptation of AC corticocollicular (Ccol) and L5B corticocallosal (Ccal) neurons are distinct. ***A***, AP waveforms of representative Ccol and Ccal neurons. Arrows indicate AP width. ***B***, On average, Ccol neurons have narrower APs (1.00 ± 0.04 ms, $n = 32$, vs 1.26 ± 0.07 ms, $n = 29$; $p = 0.0016$). ***C***, On average, Ccol neurons have a more hyperpolarized AP threshold (−40.70 ± 0.59 mV, $n = 32$, vs −36.95 ± 0.65 mV, $n = 29$; $p < 0.0001$). ***D***, Representative firing of Ccol and Ccal neurons in response to increasing depolarizing current (0–400 pA, 50 pA increments). ***E***, Firing frequency as a function of injected current amplitude for Ccal and Ccol neurons (*f–I* relationship). The slope of the *f–I* curve between 150 and 250 pA is used to calculate the slope (gain) of the *f–I* curve. ***F***, The *f–I* slope is significantly steeper for Ccol neurons (0.11 ± 0.01 Hz/pA, $n = 32$ vs 0.08 ± 0.004 Hz/pA, $n = 29$, $p = 0.0007$). ***G***, The smallest current step that elicited firing is significantly higher for Ccol neurons (162.50 ± 8.09 pA, $n = 32$ vs 131.03 ± 7.12 pA, $n = 29$, $p = 0.005$ rank sum test; numbers next to circles indicate the number of neurons that fire under this current injection). ***H***, Temporal patterning of action potential generation was analyzed by calculating instantaneous firing frequencies (i.e., inverse of the interspike interval). ***I***, Ccol neurons often start to fire with a faster initial doublet (inset, marked by the arrow) at the onset of current injection compared with Ccal neurons. Spike frequency decreases (adapts) over time in Ccal neurons while it remains nearly constant in Ccol neurons. ***J1***, ***J2***, Instantaneous firing frequency as a function of time for Ccal and Ccol neurons. Initial instantaneous frequency for Ccol neurons is high, which indicates more fast-doublet firing. Insets illustrate instantaneous firing frequency in Ccol and Ccal neurons after the initial fast doublet. ***K***, The average adaptation ratio, AR = f_9/f_2 (see ***H*** and ***I*** for representative traces), is significantly lower for Ccal neurons and close to 1 for Ccol neurons (0.70 ± 0.02, $n = 29$, vs 0.97 ± 0.03, $n = 32$, $p < 0.0001$). ***L***, The average fast-doublet index, FDI = f_1/f_2 (see ***H*** and ***I*** inset for representative traces), is significantly higher in Ccol neurons (7.50 ± 1.18, $n = 32$, vs 1.73 ± 0.09, $n = 29$, $p < 0.0001$).

relative constancy of the instantaneous firing frequency in corticocollicular neurons after the initial fast doublet (Fig. 4*J1*, inset) indicates lack of spike-frequency adaptation. Corticocallosal neurons exhibit low initial instantaneous firing frequency (Fig. 4*J2*), because they do not show fast-doublet firing. The relative decay of instantaneous firing frequency in corticocallosal neurons (Fig. 4*J2*, inset) indicates spike-frequency adaptation. Overall, corticocollicular neurons fire in a more tonic (nonadapting) pattern and corticocallosal neurons fire in a more phasic (adapting) pattern (Fig. 4*D–L*). PT neurons in mouse somatosensory cortex (S1) show greater spike-frequency adaptation than their counterparts in mouse motor cortex (M1; Miller et al., 2008); our results indicate that the AC corticocollicular neurons are more consistent with the M1 pattern, which has also been reported for PT neurons in secondary somatosensory cortex (Suter et al., 2013). Collectively, our results indicate that spiking properties of AC L5B projection neurons are cell specific and are consistent with previous *in vitro* studies suggesting that PT neurons tend to fire in a tonic pattern, and IT neurons fire in a more phasic pattern (Shepherd, 2013). Our results suggest that these

cell-specific intrinsic properties may contribute to the observed burst-like and more sustained firing in PT compared with IT L5 neurons in response to sound (Sun et al., 2013).

Unitary connections from L2/3 to L5B projection neurons

To assess synaptic properties within the AC intracortical circuits of L2/3→L5B projection neurons, we recorded from synaptically coupled pairs of L2/3→corticocollicular and L2/3→corticocallosal neurons. Connections were assessed by eliciting presynaptic spikes in the L2/3 neuron while monitoring EPSCs in the corticocollicular or L5B corticocallosal neuron (Fig. 5*A*,*B*). Connection rates were similar for L2/3→corticocollicular (14 connections found out of 235 tested) and L2/3→corticocallosal (11 connections found out of 223 tested) unitary connections. For all pairs we only tested the connectivity from L2/3→corticocollicular or L2/3→corticocallosal; we did not test for connectivity in the reverse direction. Unitary EPSC amplitude and other baseline unitary connection properties such as latency, rise time, and decay time constant were not different (Fig. 5*C*–*F*).

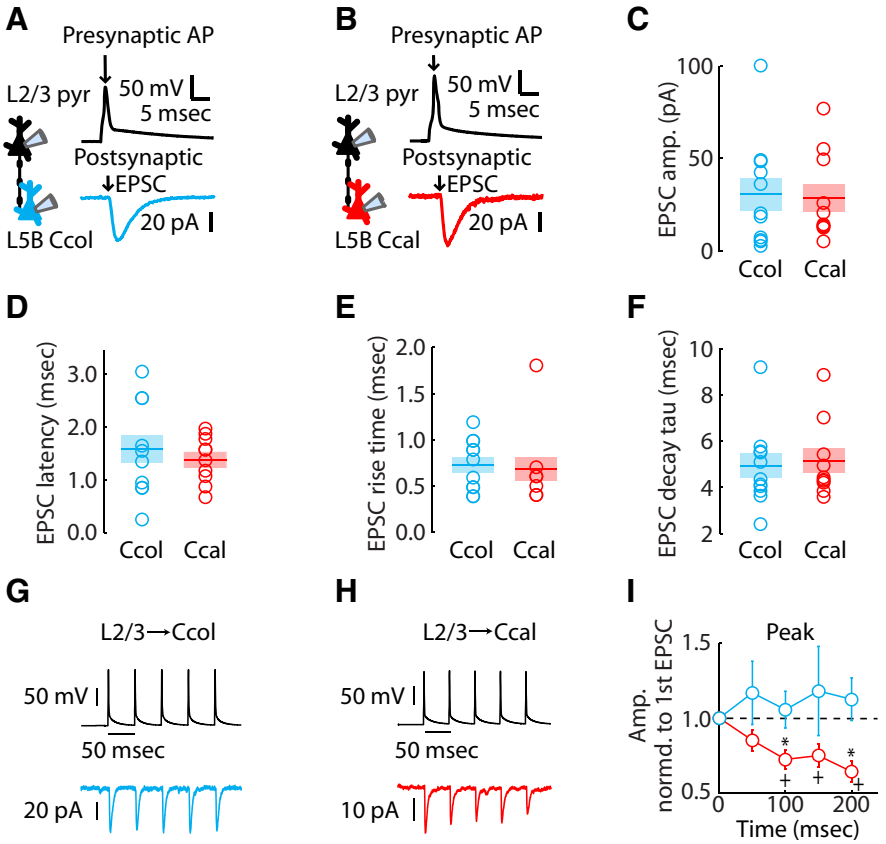

Figure 5. Paired recordings reveal similar basal synaptic properties but pathway-specific short-term plasticity of corticocollicular and L5B corticocallosal neurons; L2/3→corticocallosal connections depress, but L2/3→corticocollicular connections do not depress. ***A***, Example unitary L2/3→corticocollicular connection. ***B***, Example unitary L2/3→corticocallosal connection. ***C***, Average unitary EPSC amplitude (L2/3→Ccal = 28.90 ± 8.20 pA; L2/3→Ccol = 30.90 ± 8.80, $p > 0.05$). ***D***, Average unitary EPSC latency (L2/3→Ccol = 1.60 ± 0.30 ms, $n = 11$; L2/3→Ccal = 1.40 ± 0.10 ms, $n = 10$, $p > 0.05$). ***E***, Average unitary EPSC rise time (L2/3→Ccal = 0.70 ± 0.10 ms; L2/3→Ccol = 0.70 ± 0.10 ms, $p > 0.05$). ***F***, Average unitary EPSC decay tau (L2/3→Ccal = 5.10 ± 0.50 ms; L2/3→Ccol = 4.90 ± 0.50 ms, $p > 0.05$). ***G***, An example of AP train in presynaptic L2/3 neuron eliciting a series of EPSCs in a Ccol neuron. ***H***, An example of AP train in presynaptic L2/3 neuron eliciting an EPSC train in an L5B Ccal neuron. ***I***, Average peak amplitudes of the EPSCs in the train, normalized to the peak amplitude of the first EPSC. Asterisks indicate significant differences between L2/3→Ccol ($n = 11$) and L2/3→Ccal ($n = 10$) connections (at time = 100 ms, L2/3→Ccal = 0.72 ± 0.06, L2/3→Ccol = 1.06 ± 0.12, $p = 0.037$; at time = 200 ms, L2/3→Ccal = 0.64 ± 0.07, L2/3→Ccol = 1.12 ± 0.14, $p = 0.01$). Pluses indicate significant differences compared with the first EPSC within L2/3→corticocallosal or L2/3→corticocollicular connections (compared with the first L2/3→Ccal EPSC, at time = 100 ms, L2/3→Ccal = 0.72 ± 0.06, $p = 0.002$; at time = 150 ms, L2/3→Ccal = 0.75 ± 0.07, $p = 0.01$; at time = 200 ms, L2/3→Ccal = 0.64 ± 0.07, $p = 0.0009$).

Given the importance of short-term synaptic plasticity dynamics in sensory processing (Abbott and Regehr, 2004) and the more sustained synaptic response properties to sound in AC PT neurons (Sun et al., 2013), we hypothesized that short-term plasticity might differ between L2/3→corticocollicular and L2/3→corticocallosal synapses. Trains of action potentials at 20 Hz in the presynaptic L2/3 neuron evoked a depressing series of EPSCs in L5B corticocallosal neurons, but EPSC strength was maintained throughout the series of EPSCs in corticocollicular neurons (Fig. 5*G*–*I*). Together, our results indicate that spatially intermingled AC L5B projection neurons receive pathway-specific inputs that show distinct short-term synaptic plasticity. The cell/pathway-specific short-term plasticity of L5B corticocollicular and corticocallosal neurons favors a tonic (sustained) relay of information in the L2/3→corticocollicular pathway and a phasic (transient) relay of information in L2/3→corticocallosal pathway.

To explore the interaction of synaptic and intrinsic properties in shaping activity in corticocollicular and corticocallosal neurons, we next recorded unitary responses from the same connected pairs in current-clamp mode (Fig. 6*A*,*B*). Consistent with our paired recordings in voltage-clamp mode, current-clamp experiments revealed that baseline unitary EPSP parameters did not differ between L2/3→corticocollicular and L2/3→corticocallosal connections (Fig. 6*C*–*E*), with one exception: the decay time constant of the unitary EPSP for L2/3→corticocallosal connections was significantly longer (Fig. 6*F*). This finding is consistent with lower amounts of I_h and higher input resistance in corticocallosal neurons (Fig. 3*B*,*D*). Trains of action potentials in the presynaptic L2/3 neuron did not change significantly the peak of the unitary EPSPs in either L2/3→corticocollicular or L2/3→corticocallosal connections (Fig. 6*G*,*H*). The peak amplitude of the series of EPSPs reflects the combination of temporal summation and synaptic depression/facilitation; thus, to assess the contribution of temporal summation we measured the trough values in the EPSPs (Fig. 6*G*). Trough values were higher for L2/3→corticocallosal connections, suggesting more temporal summation for L2/3→corticocallosal connections (Fig. 6*I*). This result is consistent with the reduced levels of I_h in corticocallosal neurons (Fig. 3*D*). Subtraction of trough from the peak values (peak − trough) revealed greater values for L2/3→corticocollicular connections, suggesting that L2/3 inputs do not depress for corticocollicular neurons, but depress for L5B corticocallosal neurons (Fig. 6*J*). These results are consistent with our voltage-clamp mode experiments (Fig. 5*I*) and unmask the interaction of cell-specific intrinsic and synaptic properties in shaping the differential

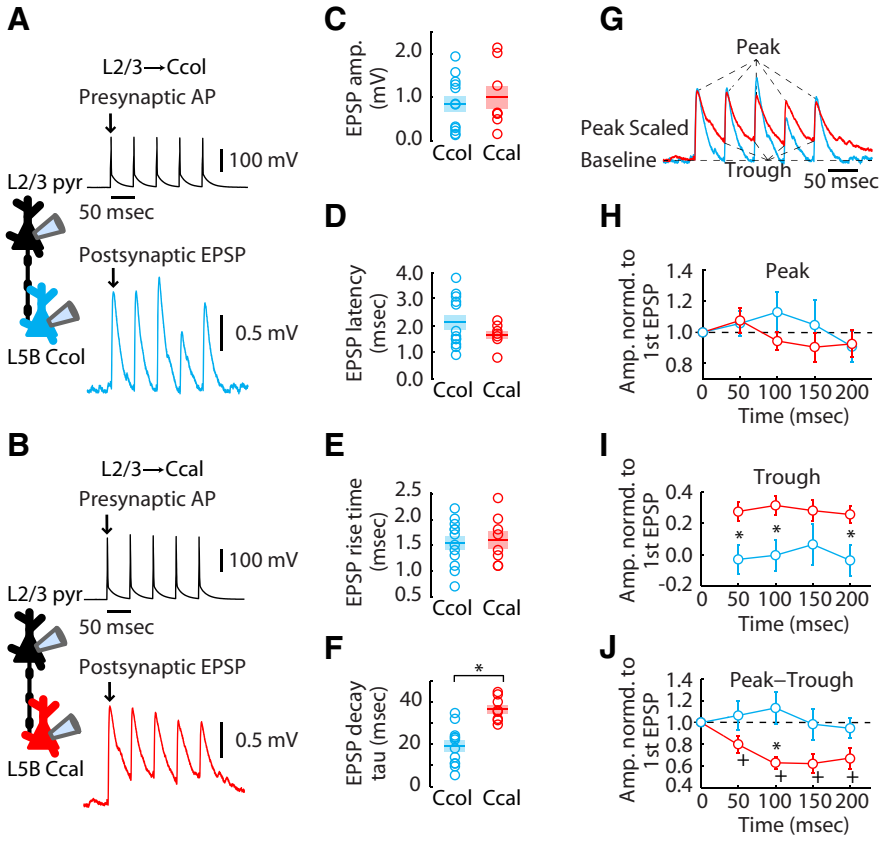

Figure 6. Synaptic dynamics of L2/3→corticocollicular and L2/3→corticocallosal connections in current-clamp mode. ***A***, Example unitary L2/3→corticocollicular connection. ***B***, Example unitary L2/3→corticocallosal connection. ***C***, Average unitary EPSP amplitude (L2/3→Ccol = 0.80 ± 0.20; L2/3→Ccal = 1.00 ± 0.30 mV, $p > 0.05$). ***D***, Average unitary EPSP latency (L2/3→Ccol = 2.10 ± 0.30 ms, $n = 11$; L2/3→Ccal = 1.60 ± 0.10 ms, $n = 8$, $p > 0.05$). ***E***, Average unitary EPSP rise time (L2/3→Ccol = 1.5 ± 0.1 ms; L2/3→Ccal = 1.60 ± 0.20 ms, $p > 0.05$). ***F***, Average unitary EPSP decay tau (L2/3→Ccol = 19.00 ± 2.60 ms; L2/3→Ccal = 36.50 ± 2.00 ms, $p = 0.0001$). ***G***, Overlay of traces from ***A*** and ***B***, normalized to the first EPSP. ***H***, Average peak amplitudes of the EPSPs in the train, normalized to the amplitude of the first EPSP. No significant differences are observed between or within groups. ***I***, Trough amplitudes, normalized to the amplitude of the first EPSP. Asterisk indicates significant differences between L2/3→Ccol and L2/3→Ccol connections (at time = 50 ms, L2/3→Ccal = 0.28 ± 0.06, L2/3→Ccol = −0.03 ± 0.09, $p = 0.024$; at time = 100 ms, L2/3→Ccal = 0.32 ± 0.06, L2/3→Ccol = 0.00 ± 0.10, $p = 0.028$; at time = 200 ms, L2/3→Ccal = 0.26 ± 0.06, L2/3→Ccol = −0.04 ± 0.1, $p = 0.039$). ***J***, Trough-subtracted peak EPSP amplitudes, normalized to the amplitude of the first EPSP. Peak–trough values were obtained by subtracting the peak amplitude of the EPSP from the trough amplitude of the preceding EPSP; this resulted in four peak–trough values at 50, 100, 150, and 200 ms. The first value at time = 0 ms is not a peak–trough value: it is the normalized amplitude of the peak of the first EPSP. Asterisk indicates significant differences between L2/3→Ccol and L2/3→Ccal connections (at time = 100 ms, L2/3→Ccol = 1.13 ± 0.15; L2/3→Ccal = 0.63 ± 0.06, $p = 0.016$). Pluses indicate significant differences within L2/3→CCol or L2/3→CCal connections. Compared with the first L2/3→Ccal peak–trough, at time = 50 ms, L2/3→Ccal = 0.80 ± 0.08, $p = 0.038$; at time = 100 ms, L2/3 →Ccal = 0.63 ± 0.06, $p = 0.0003$; at time = 150 ms, L2/3→Ccal = 0.62 ± 0.09, $p = 0.004$; at time = 200 ms, L2/3→Ccal = 0.67 ± 0.10, $p = 0.012$.

kinetics and dynamics of L2/3 synaptic inputs to corticocollicular and L5B corticocallosal neurons.

In response to L2/3 stimulation, the combined effects of synaptic and intrinsic properties shape cell-specific L5B firing

The constancy of the peak voltage of unitary EPSPs, in either L2/3→corticocollicular or L2/3→corticocallosal connections during a 20 Hz train of presynaptic action potentials (Fig. 6*G*), suggests that the spiking output of these two pathways in response to L2/3 repetitive stimulation would be similar. However, because EPSC and EPSP amplitudes (peak–trough) for L2/3→corticocallosal synapses depress (Figs. 5*I*, 6*J*), the lack of depression of the peak voltages of L2/3→corticocallosal synapses is probably due to the increased summation (Fig. 6*I*) arising from longer synaptic decay time constants (Fig. 6*F*). At lower stimulation frequencies, where summation is less or not occurring, we expect that the pathway-specific depression of L2/3→corticocallosal may reveal depression of EPSP peaks and postsynaptic firing in corticocallosal but not corticocollicular neurons.

To test this hypothesis, we investigated the effect of a lower frequency of presynaptic stimulation, 10 Hz—which generates less summation—on monosynaptic EPSPs and postsynaptic firing for L2/3→corticocollicular and L2/3→corticocallosal connections. Because the size of unitary EPSPs does not lead to firing in either corticocollicular or corticocallosal neurons, for this experiment we used extracellular electrical stimulation by positioning a stimulating electrode in L2/3 and recording EPSPs from corticocollicular and corticocallosal neurons (in the same slice); these EPSPs were larger and capable of inducing firing in both corticocollicular and corticocallosal neurons. This stimulation method presumably activated not only L2/3 pyramidal neurons but also other cell types (including interneurons mediating feedforward inhibition). However, we assume that a significant fraction of the postsynaptic responses represents inputs from L2/3 pyramidal neurons. A 20 Hz stimulation led to pathway-specific depression of L2/3→corticocallosal EPSCs similar to the one that we observed with paired recordings (Fig. 7*A–C*), suggesting that pathway-specific synaptic plasticity between L2/3→corticocollicular and L2/3→corticocallosal connections is a robust phenomenon maintained even at less stringent stimulation conditions. Importantly, 10 Hz stimulation led to similar pathway-specific depression in L2/3→corticocallosal EPSCs, while L2/3→corticocollicular EPSCs remain unaffected (Fig. 7*D–F*). Because temporal summation of EPSPs is less in 10 Hz and synaptic depression is occurring at this frequency, in current-clamp mode, we observed a depression in the peak amplitude of L2/3→corticocallosal EPSPs during 10 Hz stimulation, which was absent in L2/3→corticocollicular EPSPs (Fig. 7*G–I*). Therefore, we hypothesized that the synaptic dynamics we observe will have a differential frequency-dependent effect on the firing of the two projection neurons. Namely, 10 and 20 Hz stimulation of L2/3 is expected to lead to similar firing in corticocollicular neurons, but 10 Hz stimulation is expected to lead to decreased firing, compared with 20 Hz, in corticocallosal neurons. Consistent with our hypothesis, at threshold conditions (~50% firing in response to 10 pulses, 20 Hz stimulation protocol), transitions from 20 to 10 Hz stimulation left corticocollicular firing unaffected (Fig. 7*J*,*K*), but led to decreased firing in corticocallosal neurons (Fig. 7*L*,*M*). This is an important finding, suggesting that in AC, synaptically driven

corticocallosal output is modulated by frequency while corticocollicular output is frequency-independent.

Discussion

To characterize the synaptic and intrinsic properties of corticocollicular and corticocallosal neurons, we developed paradigms for *ex vivo* analysis of L5B projection neurons in mouse AC. Our approach was based on the combined use of retrograde fluorescent labeling to selectively label corticocollicular and L5B corticocallosal neurons, single-cell electrophysiology, and paired recordings to isolate unitary L2/3 connections to L5B projection neurons for quantitative assessment of synaptic properties. We show that sustained L2/3 activity unmasks a dynamic fractionation of the L2/3→5B pathway that generates frequency-independent firing in corticocollicular neurons and frequency-dependent firing in corticocallosal neurons. While we have not explored whether different subnetworks of L2/3 neurons project to corticocollicular and corticocallosal L5 neurons, our results are consistent with previous studies in somatosensory cortex showing that specific subnetworks in L5 receive input from different L2/3 subnetworks with distinct connection probabilities (Kampa et al., 2006). In this context, we propose that different subnetworks of L2/3→5B, with similar connection probabilities but with distinct dynamic properties, may underlie corticocallosal versus corticocollicular auditory processing.

Linking the response properties of corticocollicular and corticocallosal neurons with synaptic and intrinsic properties

AC neurons display a variety of firing behaviors in response to acoustic stimuli. Firing can range from phasic to tonic, and can vary monotonically or nonmonotonically with intensity (Volkov and Galazjuk, 1991; Schreiner et al., 1992; Calford and Semple, 1995; Barbour and Wang, 2003; X. Wang et al., 2005; de la Rocha et al., 2008). L5B contains different types of projection neurons with different response properties (Turner et al., 2005; Atencio and Schreiner, 2010a, b; Sun et al., 2013). PT- and corticocallosal-type L5B neurons in AC display dichotomous sound-evoked responses, with PT-type neurons firing in a more sustained (tonic) pattern and corticocallosal-type neurons in a more transient (phasic) manner (Sun et al., 2013).

The lack of spike-frequency adaptation (Fig. 4*I–K*), the narrower action potentials (Fig. 4*A*,*B*), and the increased gain in frequency-current relationships of

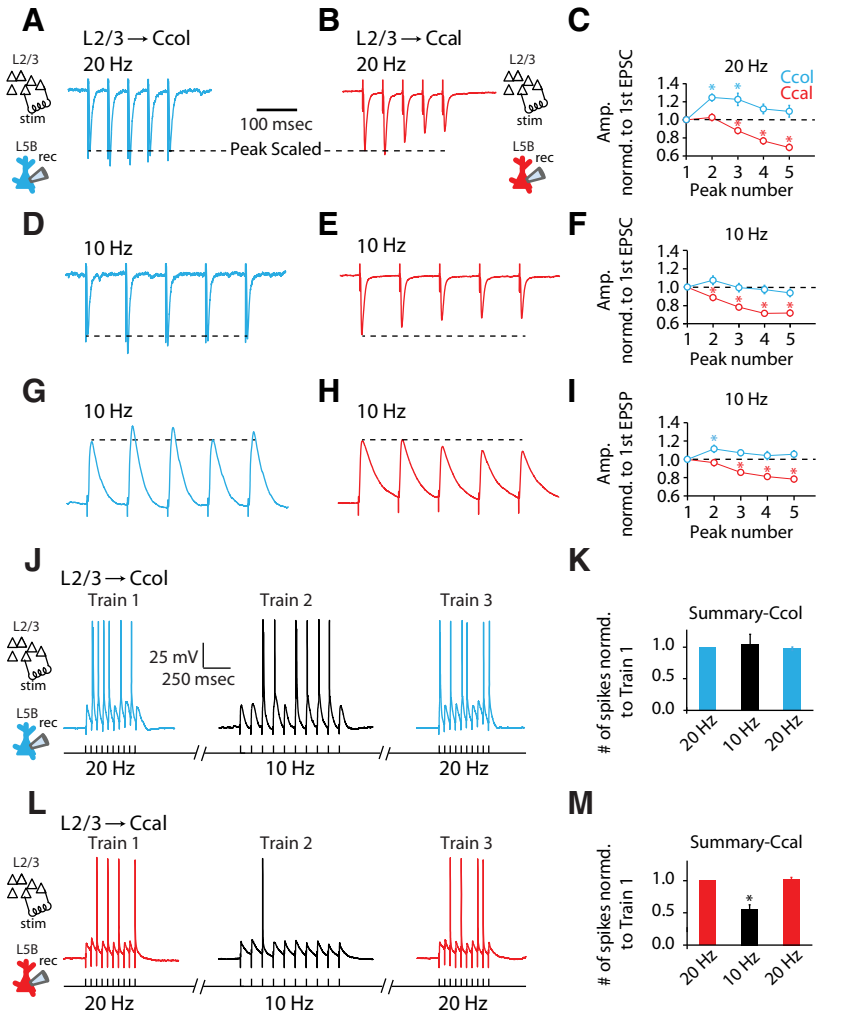

Figure 7. In response to L2/3 stimulation, the spiking of corticocallosal, but not corticocollicular, neurons is frequency dependent. ***A***, An example of an EPSC train in a Ccol neuron elicited by a train of 20 Hz extracellular stimulation of L2/3. ***B***, An example of an EPSC train in a Ccal neuron elicited by a train of 20 Hz extracellular stimulation of L2/3. Dotted line in ***A–I*** indicates normalization to first EPSC/P. ***C***, Average peak amplitudes of the EPSCs from trains as in ***A*** and ***B***, normalized to the peak amplitude of the first EPSC. Red asterisks indicate significant differences compared with first EPSC within L2/3→corticocallosal connection (compared with the first EPSC peak, at peak 3, L2/3→Ccal = 0.88 ± 0.03, $p = 0.003$; at peak 4, L2/3→Ccal = 0.77 ± 0.04, $p < 0.0001$; at peak 5, L2/3→Ccal = 0.70 ± 0.03, $p < 0.0001$; $n = 14$). Cyan asterisks indicate significant differences compared with the first EPSC peak for the L2/3→corticocollicular connection (compared with the first EPSC peak, at peak 2, L2/3→Ccol = 1.25 ± 0.04, $p = 0.0002$; at peak 3, L2/3→Ccol = 1.23 ± 0.07, $p = 0.01$; $n = 9$). ***D***, An example of an EPSC train in a Ccol neuron elicited by a train of 10 Hz extracellular stimulation of L2/3. ***E***, An example of an EPSC train in a Ccal neuron elicited by a train of 10 Hz extracellular stimulation of L2/3. ***F***, Average peak amplitudes of the EPSCs from trains as in ***D*** and ***E***, normalized to the peak amplitude of the first EPSC. Asterisks indicate significant differences compared with the first EPSC within L2/3→corticocallosal connection (compared with the first EPSC peak, at peak 2, L2/→Ccal = 0.88 ± 0.03, $p = 0.0002$; at peak 3, L2/3→Ccal = 0.78 ± 0.03, $p < 0.0001$; at peak 4, L2/3→Ccal = 0.72 ± 0.03, $p < 0.0001$; at peak 5, L2/3→Ccal = 0.72 ± 0.03, $p < 0.0001$; $n = 14$). There is no significant difference in the EPSC train for L2/3→Ccol connection ($n = 9$). ***G***, An example of an EPSP train in a Ccol neuron elicited by a train of 10 Hz extracellular stimulation of L2/3. ***H***, An example of an EPSP train in a Ccal neuron elicited by a train of 10 Hz extracellular stimulation of L2/3. ***I***, Average peak amplitudes of the EPSPs from trains as in ***G*** and ***H***, normalized to the peak amplitude of the first EPSP. Red asterisks indicate significant differences compared with the first EPSC within L2/3→corticocallosal connection (compared with the first EPSC peak, at peak 3, L2/3→Ccal = 0.86 ± 0.03, $p < 0.0001$; at peak 4, L2/3→Ccal = 0.81 ± 0.03, $p < 0.0001$; at peak 5, L2/3→Ccal = 0.78 ± 0.03, $p < 0.0001$; $n = 14$). Cyan asterisk indicates a significant difference compared with the first EPSC within L2/3→corticocollicular connection (compared with the first EPSC peak, at peak 2, L2/3→Ccol = 1.12 ± 0.04, $p = 0.01$; $n = 9$). ***J***, An example of spikes elicited in a Ccol neuron by three trains of extracellular stimulation of L2/3 (10 pulses in each train, delivered in succession at 20, 10, and 20 Hz, respectively). The breaks (//) indicate that at the end of each stimulation train, a 10 s pause was introduced before the starting the next train. ***K***, Average data for the example shown in ***J***; number of spikes fired in each train have been normalized to the number of spikes fired in the first 20 Hz train. Ccol neurons fire a similar number of spikes at 20 and 10 Hz (compared with 20 Hz train 1, at 10 Hz train 2, Ccol neurons fired an average of 1.04 ± 0.16 spikes, $p = 0.78$; 20 Hz train 1 and 20 Hz train 3 are not significantly different, $p = 0.5$; $n = 5$). ***L***, Example traces, as the one in ***J***, but for Ccal neurons. ***M***, Average data for the example shown in ***L***; number of spikes fired in each train have been normalized to the number of spikes fired in the first 20 Hz train. Ccal neurons fire significantly fewer spikes at 10 Hz compared with those at 20 Hz (compared with 20 Hz train 1, at 10 Hz train 2, Ccal neurons fired an average of 0.55 ± 0.07 spikes, $p = 0.0002$; 20 Hz train 1 and 20 Hz train 3 are not significantly different, $p = 0.5289$; $n = 6$).

corticocollicular neurons (Fig. 4*F*) suggest that the spike properties of these neurons—in accordance to their sound responses *in vivo*—allow for more reliable, sustained firing. The observed burst-like (faster initial doublet) firing in corticocollicular neurons in the presence of blockers of excitatory and inhibitory synaptic transmission (Fig. 4*I*,*L*) suggests that the intrinsic properties of corticocollicular neurons contribute to the bursting responses of PT neurons to sound (Sun et al., 2013).

The nondepressing excitatory L2/3 input to corticocollicular neurons is consistent with the *in vivo* long-lasting excitatory responses of PT neurons to acoustic stimuli (Sun et al., 2013). Given that the corticocollicular projection shapes the response properties of IC neurons, and mediates sound localization learning (Bajo et al., 2010), our results suggest that sustained activity in the corticocollicular pathway may play an important role in inducing these forms of L5-mediated, learning-induced plasticity (Bajo et al., 2010).

The firing properties and the response properties of AC L5B projection neurons are determined not only by the intrinsic and L2/3 synaptic properties studied in our experiments, but also by excitatory and inhibitory synaptic inputs arising from other local intracortical sources. In addition to L2/3, a second source of input to L5B neurons is from other L5B neurons. Based on studies from other cortical areas, L5 PT and corticocallosal neurons form recurrent (within-class) connections, but across-class connectivity, are asymmetric and in some cases even unidirectional from corticocallosal to PT neurons (Morishima and Kawaguchi, 2006; Brown and Hestrin, 2009b; Kiritani et al., 2012). If this hierarchical microcircuit organization occurs in AC L5B, which is currently unknown, it could further contribute to the dichotomous tonic/phasic activity in L5B projection neurons, because activity in corticocollicular neurons would be further sustained through recurrent connectivity without propagating to the upstream corticocallosal neurons.

Other candidate mechanisms that could also contribute to differentially regulating L5B projection neuron activity are the thalamocortical input and the inhibitory microcircuit organization of L5B. Recently, an AC circuit model was proposed based on *in vivo* evidence (Sun et al., 2013) in which fast-spiking (FS) interneurons selectively connect to PT neurons, and non-FS interneurons selectively interact with corticocallosal neurons. Moreover, the same study suggested a direct influence of thalamocortical inputs on sound-evoked activity of PT- but not corticocallosal-type neurons (Sun et al., 2013). An additional mechanism that could further contribute to the dichotomous activity in L5B projection neurons involves interneurons and is suggested by findings in M1 and prefrontal cortex: in M1 disynaptic inhibition is stronger in corticocallosal neurons compared with PT neurons (Apicella et al., 2012), while in prefrontal cortex PT neurons receive stronger feedforward inhibition (Lee et al., 2014).

Types of excitatory inputs in AC

Our findings complement and extend previous studies of AC L5 neurons and their circuit organization (Winer and Prieto, 2001). Sherman et al. propose that glutamatergic inputs can be classified as Class 1 ("driver") or Class 2 ("modulatory"; Reichova and Sherman, 2004; Lee and Sherman, 2008, 2010; De Pasquale and Sherman, 2011; Viaene et al., 2011a, b, c). Class 1 inputs have larger initial EPSPs, exhibit paired-pulse depression, and activate only ionotropic glutamate receptors. Class 2 inputs exhibit paired-pulse facilitation and activate both ionotropic and metabotropic glutamate receptors, and depression can be converted to facilitation by activation of postsynaptic mGluR2 receptors (De Pasquale and Sherman, 2012). Our results suggest that L2/3 axons, an important source of Class 1 inputs, may be further subdivided based on their projection target (corticocollicular vs corticocallosal), with distinct short-term plasticity properties.

Short-term plasticity in the neocortex

Although in a few cases facilitating excitatory connections have been described (Y. Wang et al., 2006; Thomson and Lamy, 2007; Covic and Sherman, 2011), excitatory synaptic connections between cortical pyramidal neurons are usually depressing (Atzori et al., 2001; Thomson and Lamy, 2007; Oswald and Reyes, 2008; Covic and Sherman, 2011; Reyes, 2011). Because L2/3 inputs to L5B corticocallosal neurons depress, corticocallosal output is reduced during sustained cortical activity in frequencies where temporal summation of EPSPs is reduced (Fig. 7*H*,*I*). In contrast, the lack of depression in the L2/3 to corticocollicular pathway renders the corticocollicular pathway active during sustained cortical activity, irrelevant of the frequency of presynaptic stimulation (Figs. 6, 7). Our results are consistent previous studies showing pathway-specific depression of callosal inputs to IT neurons but not in PT neurons in L5 neurons of prefrontal cortex (Lee et al., 2014). Moreover, our results are consistent with the observed depression of IT inputs to IT neurons but no depression of PT inputs to PT neurons in prefrontal cortex and motor cortex (Morishima and Kawaguchi, 2006; Kiritani et al., 2012). Together, these studies suggest that excitatory inputs to PT cells are nondepressing, while excitatory input to IT cells are depressing.

Our findings complement and extend previous cortical studies revealing pathway-specific, short-term plasticity of excitatory inputs in intracortical circuits. For example, short-term plasticity of excitatory inputs differs among L2/3→2/3, L2/3→5, and L5→5 connections (Williams and Atkinson, 2007). Our results reveal differential short-term plasticity even within the L2/3→5B pathway, which is determined by the projectional identity of the L5B neuron—the anatomical targeting of its long-range axonal branches to downstream centers. In this context, our results also extend recent studies in many cortical areas that have established that the projectional identity of cortical pyramidal neurons can be a major determinant of functional properties (Morishima and Kawaguchi, 2006; Brown and Hestrin, 2009a, b; Anderson et al., 2010; Dembrow et al., 2010; Little and Carter, 2013; Shepherd, 2013).

Together, our results identify an activity-dependent fractionation of L2/3 excitatory input into two dynamically distinct L2/3→5B pathways with specific input–output functions. This fractionation promotes sustained firing in L2/3→corticocollicular connections during different L2/3 stimulation rates and reduced firing in L2/3→corticocallosal connections during lower L2/3 stimulation rates. We propose that this functional architecture may represent a general feature of neocortical circuit design enabling divergent output channels to carry distinct information, rather than simply copies of the same signals.

References

Abbott LF, Regehr WG (2004) Synaptic computation. Nature 431:796–803. CrossRef Medline

Akintunde A, Buxton DF (1992) Origins and collateralization of corticospinal, corticopontine, corticorubral and corticostriatal tracts: a multiple retrograde fluorescent tracing study. Brain Res 586:208–218. CrossRef Medline

Anderson CT, Sheets PL, Kiritani T, Shepherd GM (2010) Sublayer-specific microcircuits of corticospinal and corticostriatal neurons in motor cortex. Nat Neurosci 13:739–744. CrossRef Medline

Apicella AJ, Wickersham IR, Seung HS, Shepherd GM (2012) Laminarly

orthogonal excitation of fast-spiking and low-threshold-spiking interneurons in mouse motor cortex. J Neurosci 32:7021–7033. CrossRef Medline

Atencio CA, Schreiner CE (2010a) Laminar diversity of dynamic sound processing in cat primary auditory cortex. J Neurophysiol 103:192–205. CrossRef Medline

Atencio CA, Schreiner CE (2010b) Columnar connectivity and laminar processing in cat primary auditory cortex. PLoS One 5:e9521. CrossRef Medline

Atzori M, Lei S, Evans DI, Kanold PO, Phillips-Tansey E, McIntyre O, McBain CJ (2001) Differential synaptic processing separates stationary from transient inputs to the auditory cortex. Nat Neurosci 4:1230–1237. CrossRef Medline

Bajo VM, Nodal FR, Moore DR, King AJ (2010) The descending corticocollicular pathway mediates learning-induced auditory plasticity. Nat Neurosci 13:253–260. CrossRef Medline

Barbour DL, Wang X (2003) Auditory cortical responses elicited in awake primates by random spectrum stimuli. J Neurosci 23:7194–7206. Medline

Brown SP, Hestrin S (2009a) Cell-type identity: a key to unlocking the function of neocortical circuits. Curr Opin Neurobiol 19:415–421. CrossRef Medline

Brown SP, Hestrin S (2009b) Intracortical circuits of pyramidal neurons reflect their long-range axonal targets. Nature 457:1133–1136. CrossRef Medline

Calford MB, Semple MN (1995) Monaural inhibition in cat auditory cortex. J Neurophysiol 73:1876–1891. Medline

Covic EN, Sherman SM (2011) Synaptic properties of connections between the primary and secondary auditory cortices in mice. Cereb Cortex 21: 2425–2441. CrossRef Medline

de la Mothe LA, Blumell S, Kajikawa Y, Hackett TA (2006) Cortical connections of the auditory cortex in marmoset monkeys: core and medial belt regions. J Comp Neurol 496:27–71. CrossRef Medline

de la Rocha J, Marchetti C, Schiff M, Reyes AD (2008) Linking the response properties of cells in auditory cortex with network architecture: cotuning versus lateral inhibition. J Neurosci 28:9151–9163. CrossRef Medline

Dembrow NC, Chitwood RA, Johnston D (2010) Projection-specific neuromodulation of medial prefrontal cortex neurons. J Neurosci 30:16922–16937. CrossRef Medline

De Pasquale R, Sherman SM (2011) Synaptic properties of corticocortical connections between the primary and secondary visual cortical areas in the mouse. J Neurosci 31:16494–16506. CrossRef Medline

De Pasquale R, Sherman SM (2012) Modulatory effects of metabotropic glutamate receptors on local cortical circuits. J Neurosci 32:7364–7372. CrossRef Medline

Doucet JR, Ryugo DK (2003) Axonal pathways to the lateral superior olive labeled with biotinylated dextran amine injections in the dorsal cochlear nucleus of rats. J Comp Neurol 461:452–465. CrossRef Medline

Doucet JR, Molavi DL, Ryugo DK (2003) The source of corticocollicular and corticobulbar projections in area Te1 of the rat. Exp Brain Res 153: 461–466. CrossRef Medline

Franklin KBJ, Paxinos G (2001) The mouse brain in stereotaxic coordinates. San Diego, CA: Academic.

Games KD, Winer JA (1988) Layer V in rat auditory cortex: projections to the inferior colliculus and contralateral cortex. Hear Res 34:1–25. CrossRef Medline

Gao WJ, Zheng ZH (2004) Target-specific differences in somatodendritic morphology of layer V pyramidal neurons in rat motor cortex. J Comp Neurol 476:174–185. CrossRef Medline

Guo W, Chambers AR, Darrow KN, Hancock KE, Shinn-Cunningham BG, Polley DB (2012) Robustness of cortical topography across fields, laminae, anesthetic states, and neurophysiological signal types. J Neurosci 32:9159–9172. CrossRef Medline

Hackett TA, Phillips DP (2011) The commissural auditory system. In The auditory cortex (Winer JA, Schreiner CE, eds), p. 117–132. New York: Springer.

Honma Y, Tsukano H, Horie M, Ohshima S, Tohmi M, Kubota Y, Takahashi K, Hishida R, Takahashi S, Shibuki K (2013) Auditory cortical areas activated by slow frequency-modulated sounds in mice. PLoS One 8:e68113. CrossRef Medline

Issa JB, Haeffele BD, Agarwal A, Bergles DE, Young ED, Yue DT (2014) Multiscale optical ca(2+) imaging of tonal organization in mouse auditory cortex. Neuron 83:944–959. CrossRef Medline

Kaas JH. (2011) The evolution of auditory cortex: the core areas. In: The auditory cortex (Winer JA, Schreiner CE, eds). New York: Springer.

Kampa BM, Letzkus JJ, Stuart GJ (2006) Cortical feed-forward networks for binding different streams of sensory information. Nat Neurosci 9:1472–1473. CrossRef Medline

Kiritani T, Wickersham IR, Seung HS, Shepherd GM (2012) Hierarchical connectivity and connection-specific dynamics in the corticospinal-corticostriatal microcircuit in mouse motor cortex. J Neurosci 32:4992–5001. CrossRef Medline

Lee AT, Gee SM, Vogt D, Patel T, Rubenstein JL, Sohal VS (2014) Pyramidal neurons in prefrontal cortex receive subtype-specific forms of excitation and inhibition. Neuron 81:61–68. CrossRef Medline

Lee CC, Sherman SM (2008) Synaptic properties of thalamic and intracortical inputs to layer 4 of the first- and higher-order cortical areas in the auditory and somatosensory systems. J Neurophysiol 100:317–326. CrossRef Medline

Lee CC, Sherman SM (2010) Topography and physiology of ascending streams in the auditory tectothalamic pathway. Proc Natl Acad Sci U S A 107:372–377. CrossRef Medline

Lefort S, Tomm C, Floyd Sarria JC, Petersen CC (2009) The excitatory neuronal network of the C2 barrel column in mouse primary somatosensory cortex. Neuron 61:301–316. CrossRef Medline

Little JP, Carter AG (2013) Synaptic mechanisms underlying strong reciprocal connectivity between the medial prefrontal cortex and basolateral amygdala. J Neurosci 33:15333–15342. CrossRef Medline

Middleton JW, Kiritani T, Pedersen C, Turner JG, Shepherd GM, Tzounopoulos T (2011) Mice with behavioral evidence of tinnitus exhibit dorsal cochlear nucleus hyperactivity because of decreased GABAergic inhibition. Proc Natl Acad Sci U S A 108:7601–7606. CrossRef Medline

Miller MN, Okaty BW, Nelson SB (2008) Region-specific spike-frequency acceleration in layer 5 pyramidal neurons mediated by Kv1 subunits. J Neurosci 28:13716–13726. CrossRef Medline

Morishima M, Kawaguchi Y (2006) Recurrent connection patterns of corticostriatal pyramidal cells in frontal cortex. J Neurosci 26:4394–4405. CrossRef Medline

Oswald AM, Reyes AD (2008) Maturation of intrinsic and synaptic properties of layer 2/3 pyramidal neurons in mouse auditory cortex. J Neurophysiol 99:2998–3008. CrossRef Medline

Reichova I, Sherman SM (2004) Somatosensory corticothalamic projections: distinguishing drivers from modulators. J Neurophysiol 92:2185–2197. CrossRef Medline

Reyes AD (2011) Synaptic short-term plasticity in auditory cortical circuits. Hear Res 279:60–66. CrossRef Medline

Schreiner CE, Mendelson JR, Sutter ML (1992) Functional topography of cat primary auditory cortex: representation of tone intensity. Exp Brain Res 92:105–122. CrossRef Medline

Sheets PL, Suter BA, Kiritani T, Chan CS, Surmeier DJ, Shepherd GM (2011) Corticospinal-specific HCN expression in mouse motor cortex: I(h)-dependent synaptic integration as a candidate microcircuit mechanism involved in motor control. J Neurophysiol 106:2216–2231. CrossRef Medline

Shepherd GM (2013) Corticostriatal connectivity and its role in disease. Nat Rev Neurosci 14:278–291. CrossRef Medline

Shepherd GM, Stepanyants A, Bureau I, Chklovskii D, Svoboda K (2005) Geometric and functional organization of cortical circuits. Nat Neurosci 8:782–790. CrossRef Medline

Shibuki K, Hishida R, Murakami H, Kudoh M, Kawaguchi T, Watanabe M, Watanabe S, Kouuchi T, Tanaka R (2003) Dynamic imaging of somatosensory cortical activity in the rat visualized by flavoprotein autofluorescence. J Physiol 549:919–927. CrossRef Medline

Slater BJ, Willis AM, Llano DA (2013) Evidence for layer-specific differences in auditory corticocollicular neurons. Neuroscience 229:144–154. CrossRef Medline

Stebbings KA, Lesicko AM, Llano DA (2014) The auditory corticocollicular system: molecular and circuit-level considerations. Hear Res 314:51–59. CrossRef Medline

Stiebler I, Neulist R, Fichtel I, Ehret G (1997) The auditory cortex of the house mouse: left-right differences, tonotopic organization and quantitative analysis of frequency representation. J Comp Physiol A 181:559–571. CrossRef Medline

Suga N (2012) Tuning shifts of the auditory system by corticocortical and corticofugal projections and conditioning. Neurosci Biobehav Rev 36: 969–988. CrossRef Medline

Suga N, Ma X (2003) Multiparametric corticofugal modulation and plasticity in the auditory system. Nat Rev Neurosci 4:783–794. CrossRef Medline

Suga N, Xiao Z, Ma X, Ji W (2002) Plasticity and corticofugal modulation for hearing in adult animals. Neuron 36:9–18. CrossRef Medline

Sun YJ, Kim YJ, Ibrahim LA, Tao HW, Zhang LI (2013) Synaptic mechanisms underlying functional dichotomy between intrinsic-bursting and regular-spiking neurons in auditory cortical layer 5. J Neurosci 33:5326–5339. CrossRef Medline

Suter BA, O'Connor T, Iyer V, Petreanu LT, Hooks BM, Kiritani T, Svoboda K, Shepherd GM (2010) Ephus: multipurpose data acquisition software for neuroscience experiments. Front Neural Circuits 4:100. CrossRef Medline

Suter BA, Migliore M, Shepherd GM (2013) Intrinsic electrophysiology of mouse corticospinal neurons: a class-specific triad of spike-related properties. Cereb Cortex 23:1965–1977. CrossRef Medline

Takahashi K, Hishida R, Kubota Y, Kudoh M, Takahashi S, Shibuki K (2006) Transcranial fluorescence imaging of auditory cortical plasticity regulated by acoustic environments in mice. Eur J Neurosci 23:1365–1376. CrossRef Medline

Thomson AM, Lamy C (2007) Functional maps of neocortical local circuitry. Front Neurosci 1:19–42. CrossRef Medline

Turner JG, Hughes LF, Caspary DM (2005) Divergent response properties of layer-V neurons in rat primary auditory cortex. Hear Res 202:129–140. CrossRef Medline

Viaene AN, Petrof I, Sherman SM (2011a) Synaptic properties of thalamic input to the subgranular layers of primary somatosensory and auditory cortices in the mouse. J Neurosci 31:12738–12747. CrossRef Medline

Viaene AN, Petrof I, Sherman SM (2011b) Synaptic properties of thalamic input to layers 2/3 and 4 of primary somatosensory and auditory cortices. J Neurophysiol 105:279–292. CrossRef Medline

Viaene AN, Petrof I, Sherman SM (2011c) Properties of the thalamic projection from the posterior medial nucleus to primary and secondary somatosensory cortices in the mouse. Proc Natl Acad Sci U S A 108: 18156–18161. CrossRef Medline

Volkov IO, Galazjuk AV (1991) Formation of spike response to sound tones in cat auditory cortex neurons: interaction of excitatory and inhibitory effects. Neuroscience 43:307–321. CrossRef Medline

Wang X, Lu T, Snider RK, Liang L (2005) Sustained firing in auditory cortex evoked by preferred stimuli. Nature 435:341–346. CrossRef Medline

Wang Y, Markram H, Goodman PH, Berger TK, Ma J, Goldman-Rakic PS (2006) Heterogeneity in the pyramidal network of the medial prefrontal cortex. Nat Neurosci 9:534–542. CrossRef Medline

Williams SR, Atkinson SE (2007) Pathway-specific use-dependent dynamics of excitatory synaptic transmission in rat intracortical circuits. J Physiol 585:759–777. CrossRef Medline

Winer JA (2006) Decoding the auditory corticofugal systems. Hear Res 212: 1–8. CrossRef Medline

Winer JA, Prieto JJ (2001) Layer V in cat primary auditory cortex (AI): cellular architecture and identification of projection neurons. J Comp Neurol 434:379–412. CrossRef Medline

Yamawaki N, Borges K, Suter BA, Harris KD, Shepherd GM (2014) A genuine layer 4 in motor cortex with prototypical synaptic circuit connectivity. eLife 3:e05422. CrossRef Medline

Yan J, Ehret G (2002) Corticofugal modulation of midbrain sound processing in the house mouse. Eur J Neurosci 16:119–128. CrossRef Medline

Yan J, Zhang Y, Ehret G (2005) Corticofugal shaping of frequency tuning curves in the central nucleus of the inferior colliculus of mice. J Neurophysiol 93:71–83. CrossRef Medline